ornl

OAK RIDGE NATIONAL LABORATORY

MARTIN MARIETTA

ORNL/TM-12945

RECEIVED
DEC 13 1995
OSTI

Modeling and Analysis Framework for Core Damage Propagation During Flow-Blockage-Initiated Accidents in the Advanced Neutron Source Reactor at Oak Ridge National Laboratory

S. H. Kim
R. P. Taleyarkhan
S. Navarro-Valenti
V. Georgevich

MASTER

DISTRIBUTION OF THIS DOCUMENT IS UNLIMITED

MANAGED BY
MARTIN MARIETTA ENERGY SYSTEMS, INC.
FOR THE UNITED STATES
DEPARTMENT OF ENERGY

This report has been reproduced directly from the best available copy.

Available to DOE and DOE contractors from the Office of Scientific and Technical Information, P.O. Box 62, Oak Ridge, TN 37831; prices available from (615) 576-8401, FTS 626-8401.

Available to the public from the National Technical Information Service, U.S. Department of Commerce, 5285 Port Royal Rd., Springfield, VA 22161.

This report was prepared as an account of work sponsored by an agency of the United States Government. Neither the United States Government nor any agency thereof, nor any of their employees, makes any warranty, express or implied, or assumes any legal liability or responsibility for the accuracy, completeness, or usefulness of any information, apparatus, product, or process disclosed, or represents that its use would not infringe privately owned rights. Reference herein to any specific commercial product, process, or service by trade name, trademark, manufacturer, or otherwise, does not necessarily constitute or imply its endorsement, recommendation, or favoring by the United States Government or any agency thereof. The views and opinions of authors expressed herein do not necessarily state or reflect those of the United States Government or any agency thereof.

DISCLAIMER

Portions of this document may be illegible in electronic image products. Images are produced from the best available original document.

ORNL/TM-12945

ENGINEERING TECHNOLOGY DIVISION

MODELING AND ANALYSIS FRAMEWORK FOR CORE DAMAGE PROPAGATION DURING FLOW-BLOCKAGE-INITIATED ACCIDENTS IN THE ADVANCED NEUTRON SOURCE REACTOR AT OAK RIDGE NATIONAL LABORATORY

S.H. Kim
R.P. Taleyarkhan
S. Navarro-Valenti
V. Georgevich

September 1995

Prepared by the
Oak Ridge National Laboratory
Oak Ridge, Tennessee 37831-8045
managed by
LOCKHEED MARTIN ENERGY SYSTEM, INC.
for the
U.S. DEPARTMENT OF ENERGY
under contract DOE-AC05-84OR21400

TABLE OF CONTENTS

Page

Table of Contents ii

List of Tables iii

List of Figures iv

Abstract 1

1 Introduction 1

2 ANS System Description 2

3 Core Damage Propagation Initiated by Flow Blockage Events 3

4 Model Description for Thermal State Evaluation 8

5 Computations and Analysis 11

5.1 Case Without Side Plates 11
5.2 Case With Side Plates 14
5.3 Effect of Fuel Melt Removal on Damage Propagation 14

6 Summary and Conclusions 18

7 References 18

Appendix A Nodal Temperature Evaluation 20

LIST OF TABLES

Page

Table 1 Severe Accident Characteristics of the ANS and Other Reactor Systems..... 2

Table 2 Summary of Core Damage Frequency of Flow Blockage Event..... 3

Table 3 Number of Damaged Plates Predicted by the Code Calculations..... 13

LIST OF FIGURES

Page

Fig. 1 Schematics of postulated flow blockage in ANS core assembly. 3

Fig. 2 Core damage propagation mode for flow blockage event. 5

Fig. 3 Nodalization for a multiple plate system. 8

Fig. 4 Assumed geometry of fuel assembly (top view) 10

Fig. 5 Initiation of plate damage propagation 11

Fig. 6 Propagation of ANS core plate damage 15

Fig. 7 Nodal temperature distribution at various time moments of the case T=620, k=190, Fa=1, h=0 (six nodes correspond to one plate). 15

Fig. 8 Average mass fraction of vaporized plates. 16

Fig. 9 Variation of node temperatures at the end of the calculations (six nodes correspond to one plate) 16

Fig. 10 Variation of molten mass fraction at the end of the calculations 17

Modeling and Analysis Framework for Core Damage Propagation During Flow-Blockage-Initiated Accidents in the Advanced Neutron Source Reactor at Oak Ridge National Laboratory

S.H. Kim, R.P. Taleyarkhan, S. Navarro-Valenti, and V. Georgevich
Engineering Technology Division
Oak Ridge National Laboratory
Oak Ridge, TN 37831-8045

Abstract

This paper describes modeling and analysis to evaluate the extent of core damage during flow blockage events in the Advanced Neutron Source (ANS) reactor planned to be built at the Oak Ridge National Laboratory (ORNL). Damage propagation is postulated to occur from thermal conduction between damaged and undamaged plates due to direct thermal contact. Such direct thermal contact may occur because of fuel plate swelling during fission product vapor release or plate buckling. Complex phenomena of damage propagation were modeled using a one-dimensional heat transfer model. A scoping study was conducted to learn what parameters are important for core damage propagation, and to obtain initial estimates of core melt mass for addressing recriticality and steam explosion events. The study included investigating the effects of the plate contact area, the convective heat transfer coefficient, thermal conductivity upon fuel swelling, and the initial temperature of the plate being contacted by the damaged plate. Also, the side support plates were modeled to account for their effects on damage propagation. The results provide useful insights into how various uncertain parameters affect damage propagation.

1. Introduction

The Advanced Neutron Source (ANS) is to be a multipurpose neutron research center and is currently in an advanced conceptual design stage at the Oak Ridge National Laboratory (ORNL). Major areas of research will include condensed matter physics, materials science, isotope production, and fundamental physics [1, 2]. The source of neutrons in the facility is planned to be a 303-MW(t) heavy-water-cooled and moderated research reactor housed in a large, double-walled containment dome and surrounded by thermal neutron beam experimental facilities. The reactor uses U_3Si_2–Al cermet fuel in a plate-type configuration. Cooling systems are designed with many safety features, including large heat sinks sufficient for decay heat removal; passive inventory control by accumulators, pools, and flooded cells; a layout that maximizes natural circulation capabilities; and fast, redundant shutdown systems. A defense-in-depth philosophy has been adopted. In response to this commitment, ANS project management initiated severe accident analyses and related technology development early in the design phase. This was done to aid in designing a sufficiently robust containment for retention and controlled release of radionuclides in the event of an accident. It also provides a means for satisfying on- and off-site regulatory requirements, accident-related dose exposures, containment response, and source-term best-estimate analyses for Level-2 and -3 Probabilistic Risk Analyses (PRAs) that will be produced. Moreover, it will provide the best possible understanding of the ANS under severe accident conditions and, consequently, provide insights for development of strategies and design philosophies for accident mitigation, management, and emergency preparedness efforts [3].

The preliminary Level 1 PRA of the ANS has indicated that the risk of core damage initiation is dominated by core flow blockage events. From a safety perspective, to investigate energetics of fuel-coolant interactions (FCIs), it is necessary to quantify the degree of core damage propagation, once initiated. This paper describes the overall framework for capturing in-core damage propagation and presents an initial model to analyze it during a postulated severe accident in the ANS reactor core. Among several possible scenarios of core damage accidents, primary emphasis has been currently placed on analyzing core damage accidents initiated by blockage of one or more coolant channels at the inlet (Fig. 1).

2. ANS System Description*

The ANS is currently in an advanced conceptual design stage. As such, design features of the containment and reactor systems are evolving, based on insights from ongoing studies. Table 1 summarizes the current principal design features of the ANS from a severe accident perspective compared with the High-Flux Isotope Reactor (HFIR) and a commercial light-water reactor (LWR). The ANS is to use uranium silicide fuel in an aluminum matrix with plate-type geometry and a total core mass of 100 kg. The power density of the ANS will be only about 2 times higher than that of the HFIR, but about 50 to 100 times higher than that of a large LWR. Because of such radical differences, high-power-density research reactors may give rise to significantly different severe accident issues. Such features have led to increased attention being given to phenomenological considerations dealing with steam explosions, recriticality, core-concrete interactions, core-melt progression, and fission-product release. However, compared to power reactor scenarios, overall containment loads from hydrogen generation and deflagration are relatively small for the ANS.

The reactor core is enclosed within a core pressure boundary tube, enveloped in a reflector vessel, that is immersed in a large pool of light water. Each assembly of the core is constructed with a series of involute fuel plates arranged in an annular array. The involute design provides uniform coolant gaps at all spanwise positions.

Table 1 Severe Accident Characteristics of the ANS and Other Reactor Systems

Parameter	Commercial LWR	HFIR	ANS
Power, MW(t)	2600	100 [a]	303
Fuel	UO_2	U_3O_8–Al	U_3Si_2–Al
Enrichment (m/o)	2–5	93	93 [b]
Fuel cladding	Zircaloy	Al	Al
Coolant/moderator	H_2O	H_2O	D_2O
Coolant outlet temperature, °C	317	69	92
Average power density, MW/L	<0.1	2.0	4.5
Clad melting temperature, °C	1850	580	580
Hydrogen generation potential, kg	850	10	12

[a] Now operating at a reduced power of 85 MW.

[b] 1992 baseline (reduced enrichment now being considered)

* The system description and all the calculational results provided in this report are based on the two-assembly core design.

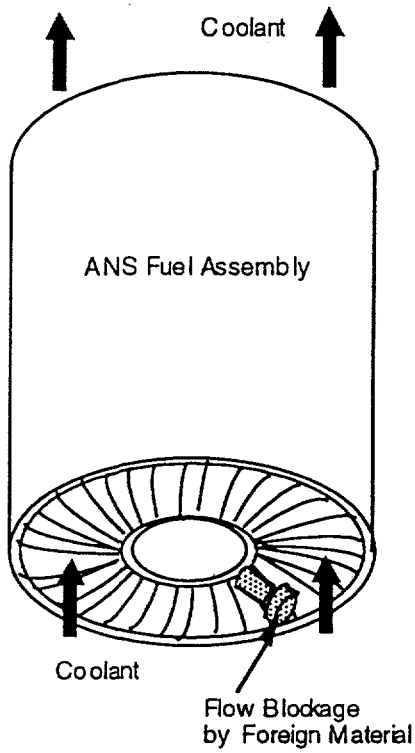

Fig. 1 Schematics of postulated flow blockage in ANS core assembly.

The fuel plate is 1.27-mm thick and consists of 0.254-mm thick 6061 aluminum cladding material sandwiching a 0.762-mm mixture of uranium silicide (U_3Si_2) and aluminum. Each coolant gap is also 1.27 mm in width and has a span of 70.29 and 87.35 mm for upper and lower core assemblies, respectively. Fuel plates are welded to inner and outer cylindrical side plates with each assembly having 507 mm of fueled length. Unfueled 10-mm leading and trailing edges are included in the fuel plates.

3. Core Damage Propagation Initiated by Flow Blockage Events

As mentioned above, the preliminary Level 1 PRA of the ANS [4] reveals flow blockage as the most probable initiating event leading to core damage. The median core damage frequency (CDF) for the event was estimated to be less than 10^{-4} per reactor year. The study divided the event into four categories, as shown in Table 2.

Table 2 Summary of Core Damage Frequency of Flow Blockage Event

Initiating Event [a]	Median Annual CDF	Percentage of Total CDF
L1 Flow Blockage	1×10^{-5}	17
L2 Flow Blockage	5×10^{-5}	56
L3 Flow Blockage	2×10^{-7}	0.2
L4 Flow Blockage	2×10^{-5}	26

[a] L1 is the event caused by debris generated in the space from the core to the inlet strainer,
L2 is the event caused by debris generated in the space from the inlet strainer to the core,
L3 is the event caused by an external debris,
L4 is the event caused by debris due to fuel manufacturing defect.

The PRA conservatively assumed that any debris items of dimension > 5 mm could initiate damage, and that about half of the potential debris sources would be larger than 10 mm. Hence, partial blockage accounts for a major portion of the risk. For each initiating event, core damage progression may be somewhat different. However, in analyzing the phenomena, the overall progression of the flow blockage event is not much different from one initiating event to the others.

Core damage propagation can follow several different paths depending on the likelihood of fuel melt removal. Figure 2 summarizes possible core damage propagation modes. As seen in the figure, core melt may either be removed (relocated) or stay at the location where the fuel plate melts. The likelihood of melt removal has not been addressed.

As demonstrated in a companion report by S.H. Kim, et. al. [5], core melt can be removed through entrainment by high velocity coolant. Coolant inertia plays a major role in sweeping fuel debris away into the coolant stream. Another possible removal mechanism is associated with a sudden expansion of water entrapped in the melt. During the process of core melting, the melt can be possibly mixed with coolant water. Such a mixture can flow along the coolant stream in a similar mode to melt entrainment. However, water entrapped in the melt globule can vaporize quickly. Consequently, an increased channel pressure may result in blowing the melt debris out of the core assembly. In this case, the debris particles, whose velocity is high enough to overcome the pressure imposed by in-coming coolant, can be dispersed into the coolant upstream as well as downstream. Also, fuel melt could candle down toward the core bottom if the inlet coolant flow is not sufficiently large.

Molten portions of fuel might also stay inside the core assembly without being removed. During normal operation, a pressure drop of about 1.5 MPa is imposed across coolant channels from inlet to exit. At the same time, however, along with significant structural deformations between the unfueled inlet and exit sections of the core, it is possible for the coolant with significant voids to be superheated and pressurized quickly in a (fully or partially) blocked channel high enough to compensate or overcome the nominal pressure drop across the channel. In this case, the melt may not be removed from its originating place. Consequently, the course of damage propagation will change if the melt contacts the adjacent fuel plate. If no contact is made, the damage can propagate to the next plate through convection and radiation of heat from the melted plate. This case is possible only when the magnitude of fuel swelling is limited or none. There are several modes in which fuel melt can contact its neighboring plate . Plate bowing due to thermal and/or mechanical stress is a possible cause of local plate contact. With a rapid evolution of fission product vapor in the fuel matrix, molten fuel could swell sufficiently to fill the coolant gap and connect with the neighboring plate. Also, debris expansion because of internal pressurization of coolant channel can cause bridging to the next plate.

As explained above, the possibility of in-core melt propagation cannot be ruled out. The current study has focused on the damage propagation mode without fuel melt removal to make conservative estimates for energetic FCI calculations. However, the effect of melt removal on the extent of damage propagation is also addressed. Fuel at the end of the cycle is assumed to contain substantial amounts of volatile fission products. Direct thermal contact between fuel plates upon fuel plate swelling, as fission product vapor is released, is a conservative assumption for enhanced damage (melting) propagation.

Several initiating events can cause the coolant channel blockage, and substantial efforts are being made by the ANS project to characterize the blockage, including evaluation of thermal-hydraulic parameters for such an event. In any case, once a coolant channel is sufficiently blocked, the affected fuel plates will experience a reduction or loss of heat

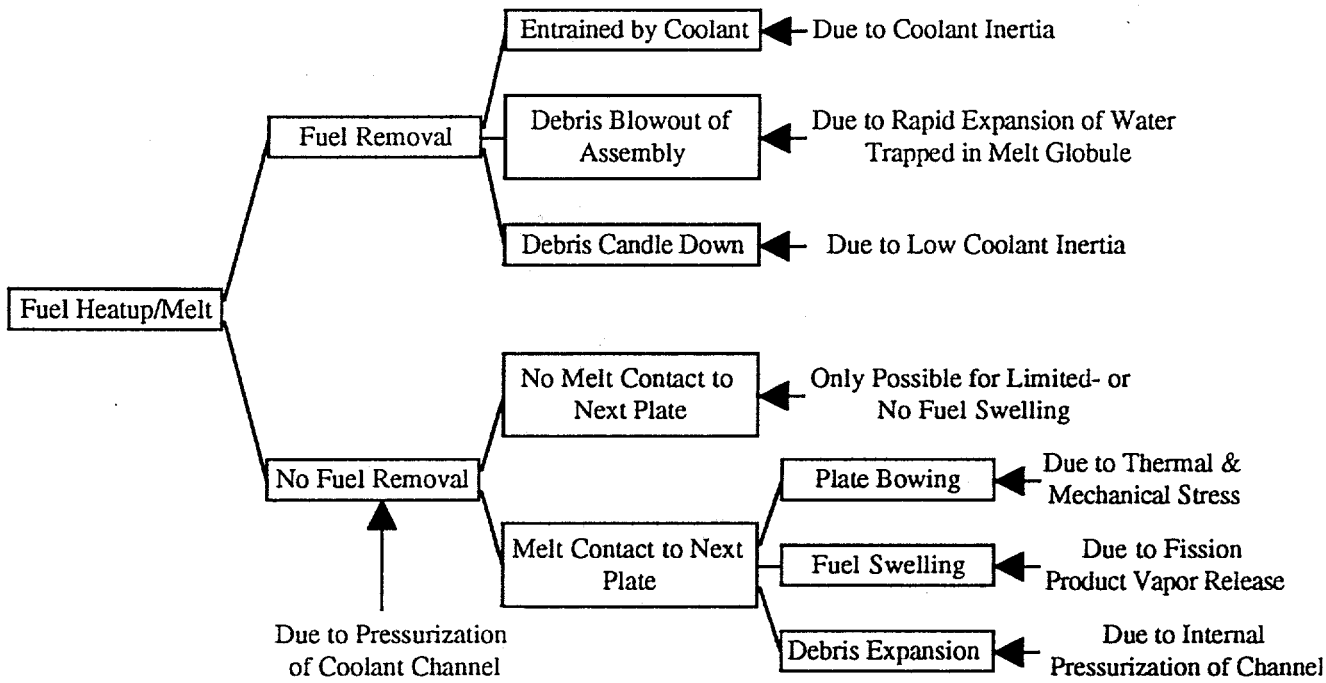

Fig. 2 Core damage propagation mode for flow blockage event.

removal. These plates will necessarily heat up to a temperature for fuel swelling to begin due to the rapid release of fission product vapors in addition to the temperature-induced volumetric expansion. Upon being contacted by such a hot damaged plate, a neighboring plate will start to heat up, become deformed, and eventually attack its other neighboring plate. Such fuel damage would propagate until an overall balance between heat generation and cooling is met. Such a heat balance may be established either by drop in fission energy following a successful reactor scram or by sufficient coolant flow provided for the plate cooling. Various configurations for the blockage are possible. Since a front-end condition for the blockage is still under investigation, however, the blockage is assumed in a way to lead to the most conservative consequences (assuming absence of localized steam explosion loads). In the current study, both coolant channels of the plate under consideration (e.g., left and right sides of the plate) are assumed to be blocked with a magnitude to reduce the coolant flow to a low enough level to cause plate damage. A constant heat transfer in other coolant channels is assumed and changed as a parameter to study the effect of heat transfer coefficient on plate damage propagation. Results of this study will be used to evaluate maximum possible energetic loads due to FCIs (described in the paper by R.P. Taleyarkhan, et al.[6]). Therefore, the temperature of the plate melt as well as its mass involved in the damage propagation need to be evaluated.

Limited work was attempted in the past for understanding damage propagation in ANS-type core under flow blockage conditions [7,8,9]. This work was attempted for HFIR conditions and did not account for some of the essential physics of core melt propagation. For example, Cole et al. estimated maximum credible damage propagation based upon reactivity insertion and other considerations [7]. Kirkpatrick utilized a simplified lumped parameter approach wherein temperature gradients within melted plates are not considered, and the melt temperature is not permitted to rise above aluminum melting [8]. Freels utilized RELAP5 to investigate melt propagation, once again, not including effects such as fuel plate temperature rise beyond melting temperature of aluminum (viz., melt superheat), thermal gradients within the melted agglomerate of fuel plates, upflow of

coolant, and thermal heat transfer to the side plates [9]. These models also do not permit sensitivity studies to evaluate effects of foamed fuel thermal conductivity changes, effects of variable contact areas of foams and undamaged fuel plates, etc. As such, although useful insights were drawn, these models lack much of the essential physics of core damage propagation-related melting-freezing thermal hydraulics, fuel behavior, as also the unique neutronic (e.g., void-reactivity coupling) behavior of the ANS core. Therefore, the above-mentioned models of Cole, Kirkpatrick and Freels are considered excellent pioneering work, but not totally adequate for ANS core damage propagation studies in support of current-day safety certification.

Several assumptions employed for the current study are described below.

Assumptions

- The core assembly is assumed to be represented by one-dimensional multiple layers of rectangular plates separated by coolant channels. It is evident that the plate melting/relocation and damage propagation have multi-dimensional aspects. However, for initial scoping estimates, such a one-dimensional treatment should provide a conservative estimation of the plate damage propagation, assuming that the core material, once it is damaged/melted, does not transport to other places, nor can it be disrupted by any external forces like coolant flow. In reality, unless the coolant channel is completely blocked, a damaged plate may possibly be swept by a high velocity coolant, and further damage propagation may be prevented. One other possible scenario is that the damaged plate mixed with coolant may trigger a local steam explosion that affects the integrity of its neighboring plates. This local steam explosion may be strong enough to disrupt the plates in neighboring channels, and/or fragments blocking other coolant channels will possibly lead to another local steam explosion. If a local steam explosion does not occur and the damaged plate mass stays there, then a thermal wave will keep propagating to heat-up the next plate. At some point of the propagation, more mass that is much hotter may be involved in a more extensive steam explosion. Currently, however, it is assumed that such a local steam explosion does not occur until the damage propagation is complete. Here, the term "propagation completion" means the end of the transient calculation due to a successful reactor scram. Even after the reactor scram, fission product decay heat would be available as a heat source. However, it is evident that such an amount is not sufficient to sustain rapid plate melting and propagation. Therefore, a transient calculation has been performed only until successful reactor scram. Initial estimates indicate that this time frame is about 4 s.

- Uniform material properties are assumed such as thermal conductivity, specific heat, and no thermal expansion (i.e., constant density). Although these properties change as a function of temperature (e.g., 10~20% for temperature range we are interested in), we assume they are constant. For future development of more detailed mechanistic models, we plan to include temperature dependency of these properties. Also, uniform constant heat generation is assumed. Data used for the calculations are given below.

κ (thermal conductivity)	=	190	W/m-K
c_p (specific heat capacity)	=	1000	J/kg-K
Q (rate of heat generation)	=	303	MW
m (total fuel and aluminum mass)	=	100	kg
Δz (channel length)	=	0.507	m
δ (plate/coolant channel thickness)	=	1.27	mm
w (plate width)	=	87.7	mm

T_{mlt} (melting temperature)	=	853	K
h_{mlt} (latent heat of fusion)	=	397	kJ/kg
T_{vap} (vaporization temperature)	=	2767	K
h_{vap} (heat of vaporization)	=	10.8	MJ/kg
T_{init} (plate initial temperature)	=	388	K

A_{cont} = f_{cont} w Δz (where f_{cont} is the fraction of surface area between nodes that intimately contact during fuel foaming)

Total number of fuel plates = 684 (432 and 252 plates for upper and lower core assemblies, respectively)

- Fuel meat and clad are assumed to be perfectly mixed and represented by one average material with the density of 2,589 kg/m^3. This density is evaluated based on 100 kg of core mass occupied by the volume of 684 plates with 0.507 m of plate length, 1.27 mm of plate thickness and 87.7 mm of plate width.

- Plate material is assumed to have one melting temperature (i.e., 853 K) and one vaporization temperature (i.e., 2,767 K). Thus, once a phase change occurs, its temperature remains constant until the phase change is complete.

- Constant reactor power is assumed during damage propagation; that is, reactivity feedback effects are ignored.

- Instead of calculating parameters to determine coolant characteristics such as coolant temperature, pressure, void fraction, and heat transfer coefficients, we assume a constant heat transfer coefficient and coolant temperature throughout the transient.

- It was assumed that the plates are not deflected due to external forces such as pressure difference between inner and outer surfaces of the affected plate.

- In a blocked channel, there is no heat sink, and thus no heat transfer is permitted from the plate surface to this coolant channel; that is, instantaneous flashing of the coolant is assumed if the channel is blocked.

- When a fuel plate reaches its melting temperature, it immediately slumps against its neighbor to the outside and blocks the coolant channel. This is assumed to be due to plate swelling caused by coalescence of fission product vapors from the fuel matrix near its melting temperature. A preliminary study shows that the fuel swelling magnitude at the end of the cycle upon fuel melting is large enough to fill the coolant gap. Any portion of the plate filling the coolant channel is assumed to be at its melting temperature. Mass of swelled nodes is reduced to one half of the original mass to ensure mass conservation.

- It was assumed that the vaporized fuel plates remain in their original locations or regions. It is realized that at this high temperature, the results become suspect. However, we already do not consider several possible physical processes to determine not only plate thermal state but also the structural behavior, mainly caused by exothermic chemical reaction between aluminum and water (i.e., ignition). This assumption is recognized as being bounding in nature, and was made to allow this scoping study to proceed.

4. Model Description for Thermal State Evaluation

A transient one-dimensional heat conduction equation describes heat transfer in fuel plates in the thickness direction, and is given by

$$\frac{\partial}{\partial t}\left(\rho\, c_p T\right) = \kappa \frac{\partial^2 T}{\partial x^2} + q''' \tag{1}$$

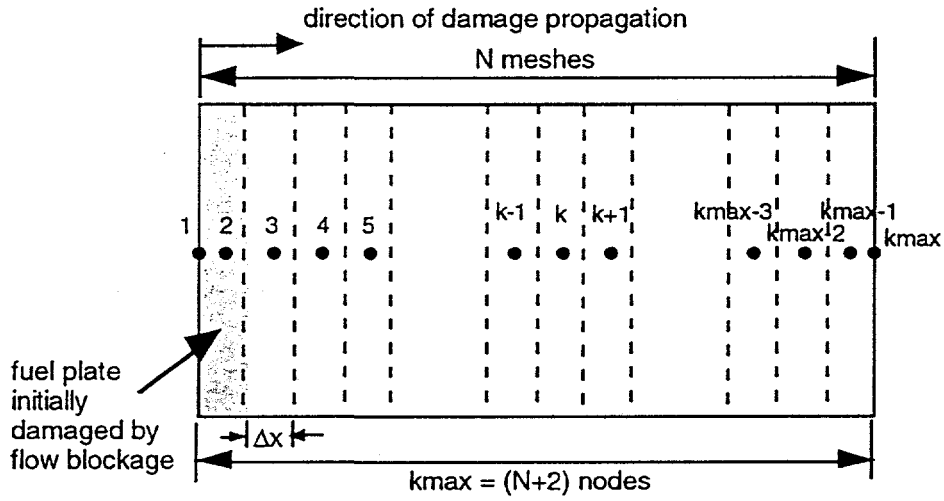

Fig. 3 Nodalization for a multiple plate system.

The numerical procedure for solving Eq. (1) involves coupled, implicit difference algorithms that apply a quasi-linearization technique, as appropriate, to ensure a stable solution of the resulting algebraic equations [10]. Numerical estimates of heatup characteristics for the plates are obtained by means of implicit finite-difference approximations to the governing conservation equation, Eq. (1).

Each set of plates under consideration is uniformly subdivided into N meshes. A nodal point is designated at the center of each mesh. In addition, to evaluate plate surface phenomena, a node with zero mass is assigned at each boundary. Therefore, a set of plate system will have (N+2) nodes. The number of plates under consideration changes as damaged plates increase. Figure 3 illustrates nodalization.

For an arbitrary node k of mass m_k and temperature T_k, the difference approximation to Eq. (1) over a time interval t-Δt to t is taken as

$$\frac{\left(mc_p\right)_k}{\Delta t}\left(T_k - T_k^*\right) = C_{k-1,k}\left(T_{k-1} - T_k\right) + C_{k,k+1}\left(T_{k+1} - T_k\right) + Q_k \tag{2}$$

A superscript ' * ' denotes a value evaluated at the previous time step. Equation (2) is rearranged as successive back-substitution for nodes k= kmax-1,kmax-2,....., 1 (the details are given in Appendix A), resulting in the final form for T_k as

$$T_k = D_k^* T_{f,L} + E_k^* T_{f,R} + F_k^* \tag{3}$$

Equation (3) with appropriate boundary conditions describes the temperature distribution of plates. It is apparent that from Eq. (3), D_k^* and E_k^* must be zero and F_k^* becomes the same as the melting or vaporization temperature of node-k if the kth node undergoes phase change as melting/freezing or vaporization/condensation.

Each node may be heated up to its melting point or the melt may undergo freezing because of net heat loss to neighboring plates and/or bulk coolant. When a nodal temperature first crosses the melting point (over- or under-shooting in the temperature is expected due to a finite size of a time step), the nodal temperature is reset to the melting temperature, and the excess energy is used to calculate the mass of material that changes phase. Therefore, the amount of the melt in node k when T_k first crosses the melting temperature (i.e., overshoots) is evaluated as

$$m_{m,k} = \frac{(m c_p)_k (T_k - T_{m,k})}{\lambda_k} \tag{4}$$

where $T_{m,k}$ and λ_k are the melting temperature and the latent heat of fusion of the kth node, respectively. In subsequent time steps, the amount of the melt in node k is evaluated as

$$m_{m,k} = m^*_{m,k} + \frac{Q_k \Delta t}{\lambda_k} \tag{5}$$

where $m^*_{m,k}$ is the molten mass at the previous time step.

Once the kth node becomes completely molten, its temperature starts to increase until it reaches the temperature for the next phase change (e.g., vaporization/condensation). Such a temperature change is again described by Eq. (3), and subsequent vaporization/condensation can be described by a similar expression as in Eqs. (4) and (5).

Since the numerical algorithm employed in the current study utilizes a fully implicit finite difference representation of Eq. (1), the solution is unconditionally stable and expected to yield a truncation error of $O[\Delta t, (\Delta x)^2]$. Our difference representation for this marching problem provides an acceptable solution to Eq. (1) because it meets the conditions of consistency and stability [11]. To examine modeling and coding errors, extensive validation and verification work was performed. It included a comparison between the results from our finite difference formulation and analytical calculations. Also included was a comparison between our results and those obtained from the well-known HEATING7 code [12]. All the cases that we examined revealed that the current formulation is quite acceptable with 3 nodal points for a single plate and time step less than 1 s. This is also true even for a very stiff problem such as sudden contact of hot melt with a cold plate. For a sample comparison against results from HEATING7, our model predicted very close results even with much more coarse nodalization (e.g., 1 node in our formulation versus 10 nodes in HEATING7 representation) and with larger time step (e.g., 0.1 s in our formulation versus 0.01 s in HEATING7).

Heat Conduction to Side Plates

Fuel plates in the ANS core span between supporting cylinders. Heat conduction to side plates may delay the damage propagation. If the side plate fails, additional flow blockage

may be provided due to transport of fragments originating from the lower assembly to the upper assembly. The geometry assumed for the calculations is given in Fig. 4.

A side plate is nodalized into the same mesh size as a connected fuel plate; that is, if each plate is nodalized into three meshes, three meshes are provided for a section of the side plate connected to the fuel plate and another three for a section facing the coolant channel. Heat transfer between the side plate meshes was neglected because it is

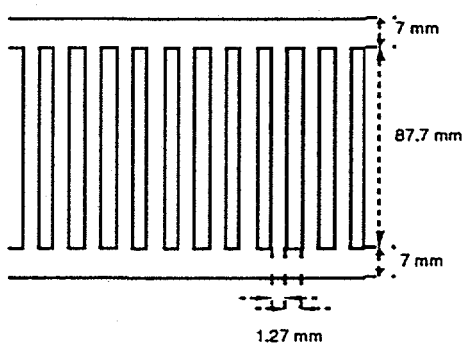

Fig. 4 Assumed geometry of fuel assembly (top view).

expected to be much smaller than that between the fuel plate and the side plate. Also, neglected was heat loss to the surrounding coolant because the side plate is expected to be covered by the steam blanket quickly once it heats up. Therefore, the nodal temperature of the side plate is given by

$$T_{k,c} = T^*_{k,c} + \frac{q''_k A_c \Delta t}{\rho_c (\Delta x\, z\, L)_c\, c_{p,c}} \tag{6}$$

where

subscript c = side plate
$T^*_{k,c}$ = temperature of node-k at the previous time,
ρ_c = density (2,700 kg/m^3),
Δx = mesh thickness,
z = mesh width (7 mm),
L = cylinder length (0.507 m),
$c_{p,c}$ = specific heat capacity (1,000 J/kg-K),
A_c = thermal conduction area (Δx L),
Δt = time step, and

q''_k is heat flux coming in from fuel plate given by

$$q''_k = \frac{\kappa}{\delta_c}\left(T_k - T_{k,c}\right) \tag{7}$$

where

κ = thermal conductivity (190 W/m-K)
δ_c = thermal conduction layer
[e.g., (z + 0.5*fuel plate width)/2 = 25.4 mm]
T_k = fuel plate temperature of node-k

When it is heated up to the melting temperature (853 K), the mesh undergoes phase change as the fuel plate does. In reality, the size of the inner cylinder is different from that of the outer cylinder. However, as seen in Fig. 4, the geometry of the cylinder including the fuel plate is assumed to be rectangular. Therefore, a representative side plate is the same for both inner and outer cylinders. For these initial calculations, therefore, only one (averaged) side plate is included.

5. Computations and Analysis

5.1 Case Without Side Plates

A scenario for fuel plate melting and propagation is depicted in Fig. 5. In these calculations, no side plates were assumed. As seen in the figure, the plate in blocked channels undergoes heatup. When the plate temperature reaches 853 K, which is the solidus temperature of AL-6061, a rapid release of fission product vapors in the fuel matrix leads to a volumetric expansion of the plate (swelling) [13]. This expanded plate will fill the adjacent coolant gap and directly contact the next plate. When expanded, the nodal mass of the swelled plate is assumed to be reduced to half of its initial mass. Here, for convenience, let us call the swelled plate plate-1, and a new intact plate being touched by the swelled plate is called plate-2.

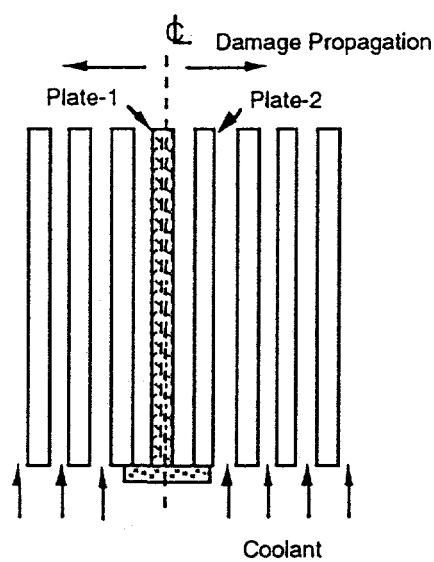

Fig. 5 Initiation of plate damage propagation.

When contacted by the hot swelled plate material, the initial temperature of plate-2 will not be same as that of plate-1 before the event was initiated. This is because plate-2 must have been heated up by convection and radiation from plate-1 before the contact. Also, if flow to this coolant channel were already affected by onset of flow excursion instability, the temperature of plate-2 should already have increased due to lack of sufficient cooling. However, at this stage the transient variation has not been modeled. Instead, a parametric analysis was done to gage the relative impact by changing the initial temperature of plate-2. One value used for the calculations was selected to be the initial temperature of plate-1 (e.g., 388 K). The other value was selected as an average of the plate-1 initial temperature and the plate melting temperature (e.g., 620.5 K).

Another uncertain parameter is the thermal conductivity of the plate. Once the plate swells, its volume is assumed to increase by a factor of two so as to fill the coolant space. Therefore, the void volume in the plate is bounded at 50%. The volume of U_3Si_2 fuel in the plate is about 11%. Under the condition of the plate expansion, the fuel particle volume will be half of 11%. Therefore, total volumetric fraction of the void and fuel will be about 56% (i.e., 50% + 11% / 2). According to the Ref. [14], thermal conductivity of such a configuration for U_3Si_2 fuel is about 20 W/m-K at 60 °C. Furthermore, Ref. [14] states that the fission gas bubbles will reduce the thermal conductivity further. Therefore, a parametric study has been performed using the constant value of 190 W/m-K all the way through the transient and with a reduced value of 10 W/m-K upon plate swelling.

The thermal conduction area is another uncertain parameter. Upon the plate swelling and mixing with voids in the coolant channel, the effective thermal conduction area will be reduced to about one-half. This is because we assume that the molten plate swells to also occupy the coolant space, the volume of which is the same as that of the plate. Hence, an effective contact area between plates will be likely reduced to ~50% since the melted plate upon swelling due to fission product gas agglomeration fills a volume that is twice the original plate volume. However, the effective heat conduction area also needs to account for heat conduction through the voids filling with hot gas (e.g., volatile fission products). Therefore, the calculations have been performed using two different thermal conduction areas between nodes in the swelled region: one for no change of the area from its initial value, and the other for the area reduced in half.

The next uncertain parameter is the convective heat transfer coefficient at unblocked coolant side of plate-2. As mentioned above, configurations for the coolant channel blockage are complex. For example, only a single channel might be completely or partially blocked, or multiple channels might also be completely or partially blocked. Because all the coolant channels are in parallel and connected with the same inlet and outlet plenums, channel blockage will possibly cause a flow excursion if the pressure drop in some channels is different from that of others caused by a significant void generation. Therefore, such a dynamic nature of the coolant thermal-hydraulics needs to be analyzed to correctly define heat transfer between plates and coolant. If a coolant channel experiences flow excursion, heat transfer from the heated plate surface to the coolant will be significantly affected. In the absence of a detailed study, the convective heat transfer coefficient at plate-2 is also varied as a parameter to investigate the plate damage propagation. Considering a possible extensive flow excursion and corresponding flashing in the affected channels, it may be conservative to choose a value corresponding to zero heat transfer to the coolant.

The reactor protection system takes a finite time (~4 s) to detect abnormality resulting from presence of fission products in the coolant downstream, and also respond to shut down the reactor. A transient time of 4 s, therefore, was selected as the time frame for plate damage propagation. Full reactor operating power (e.g., 303 MW(t)) is assumed during this period. Calculations were not extended further beyond 4 s since the ANS system has been designed to have enough capability to remove fission product decay heat by natural circulation mode after reactor shutdown.

Figures 6 through 8 show selected results of the calculations with the parametric variations described above. Table 3 also lists the number of fuel plates involved in damage propagation. As seen in Fig. 6, the plate damage propagation strongly depends on each of the parameters we examined. The case of no heat transfer to the coolant with full conduction area and high initial contact temperature (in the figure, this case is shown as T=620, k=190, a=1) yields the largest number of damaged plates (e.g., 202). With a

reduced thermal contact area of 50% (in the figure, T=620, k=190, Fa=0.5) , the number of damaged plates comes down to 174. Also, Fig. 6 shows that thermal conductivity affects the damage propagation. As the conductivity is lowered, the damage propagation becomes slower. Good estimation of the initial temperature of plate-2 is also important in precisely determining the damage propagation. Figure 6 also shows that the fuel plate damage does not propagate further if sufficient cooling can be provided for plate-2. With a heat transfer coefficient of 52 kW/m^2-K, none of the cases shows damage propagation. The average heat transfer coefficient at fuel plate surface is expected to be around 100 kW/m^2K during normal operating conditions. According to the data collected from experiments performed at the Flow Blockage Test Facility (FBTF), this heat transfer coefficient drops to ~20-40 kW/m^2K for 25% edge blockage, and ~50 kW/m^2K for 35% center blockage [15]. The heat transfer coefficient of 52 kW/m^2K evaluated by the current model for limiting the damage propagation, needs to be investigated further.

Figure 7 shows nodal temperature variations as a function of time for the case of no heat loss to the coolant with full contact area and high initial temperature of plate-2 (for which 600 nodes correspond to about 100 plates). It is seen that in about 1.2 s of the transient, inner nodes start vaporizing. A large number of nodes in melted plates experience vaporization during the transient. Such a condition could likely initiate an energetic FCI (as described in a paper by V. Georgevich, et al. [16]). This phenomenon, nevertheless,

Table 3 Number of Damaged Plates Predicted by the Code Calculations

h (W/m^2K) [a]	388-10-0.5 [b]	388-190-1 [b]	620-10-0.5 [b]	620-190-1 [b]	620-190-0.5 [b]
0.00×10^0	64	123	116	202	174
5.00×10^3	56	112	98	182	154
1.00×10^4	48	102	78	158	132
1.50×10^4	40	92	58	134	110
2.00×10^4	30	82	38	102	80
4.00×10^4	12	64	12	74	54
5.00×10^4	2	48	2	56	44
5.04×10^4		46		54	
5.08×10^4		46		52	
5.12×10^4		42		50	
5.16×10^4		40		46	
5.18×10^4		34		42	
5.20×10^4		2		2	2

a Convective heat transfer coefficient

b Case description:

Case	T	k	Fa
388-10-0.5	388	10	0.5
388-190-1	388	190	1
620-10-0.5	620	10	0.5
620-190-1	620	190	1
620-190-0.5	620	190	0.5

where T is initial temperature of plate-2 (K), k is thermal conductivity of swelled plates (W/m-K), and Fa is fractional contact area upon fuel swelling.

is conservatively excluded from consideration in the present work. However, none of the nodes at the end of the calculations is completely vaporized. The average fraction of the mass that is vaporized, is shown in Fig. 8. This fraction was averaged over the entire damaged plates at the end of the transient. The fraction, as seen in the figure, seems to depend only on convective heat transfer at plate-2. All the cases show a similar vaporization fraction. Even the case of the slower damage propagation (e.g., T=388, k=10, Fa=0.5) shows a similar fraction. However, that case reveals a higher vaporization fraction in inner nodes.

5.2 Case With Side Plates

The case "620-190-1" was used as a base for this calculation. This case assumes that the second plate temperature is 620.5 K before it contacts slumping fuel plate melt, the thermal conductivity is 190 W/m-K, and a full thermal contact area exists between plates. This case represents a worst case that conservatively estimates 202 plates to be damaged during 4 s of the transient period. This case has been repeated here along with the model of side plates. The number of damaged fuel plates was estimated as 202, which is the same as the original case without accounting for the side plates. However, average mass fraction of vaporized fuel plate was reduced from 0.32 to 0.28, which is equivalent to 11.6 MJ. This amount of energy is transferred to heat up and melt the side plates.

Other results are depicted in Figs. 9 and 10. Figure 9 shows temperature variations along the nodes at the end of the calculations (e.g., 4 s). Node-0 corresponds to the location where the damage started propagation. As seen, the side plate is heated up substantially. The number of cylinder nodes experiencing melting is about 450 nodes, which is equivalent to 7.3 kg total, accounting for symmetry of the propagation and duplex cylinders. Figure 10 shows the molten mass fraction of each node at the end of the calculations.

5.3 Effect of Fuel Melt Removal on Damage Propagation

One of most crucial assumptions employed in above calculations is that the molten fuel cannot be relocated or removed from its originating location. In reality, there might be other situations involved with fuel relocation or dispersal. In those cases, it is

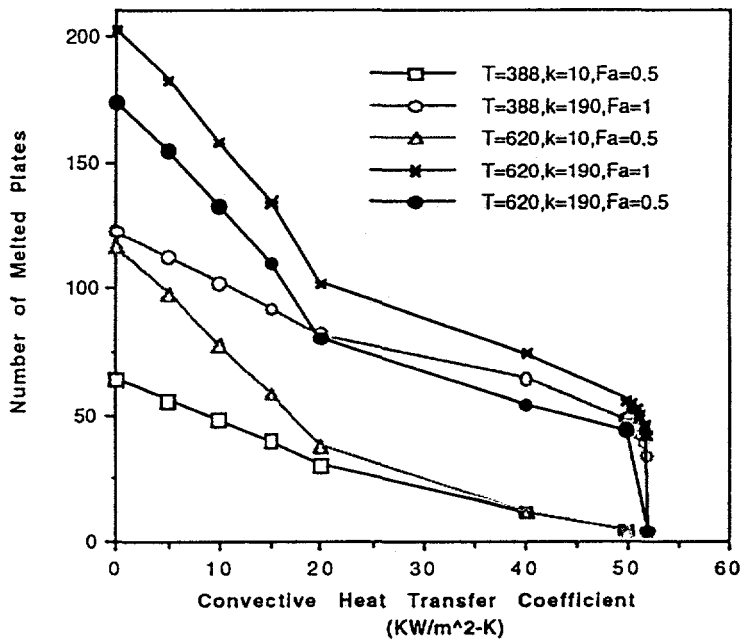

Fig. 6 Propagation of ANS core plate damage.

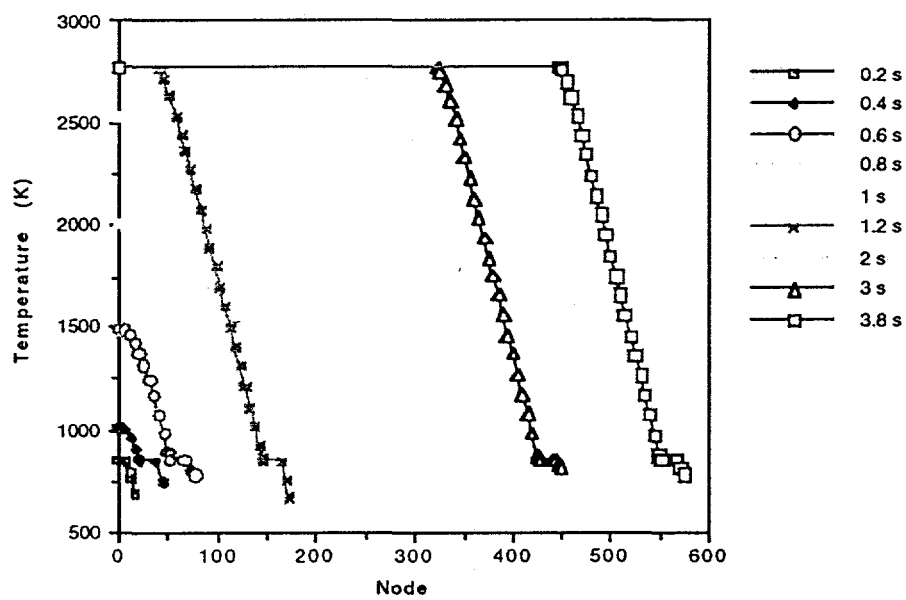

Fig. 7 Nodal temperature distribution at various time moments of the case T=620, k=190, Fa=1, h=0 (six nodes correspond to one plate).

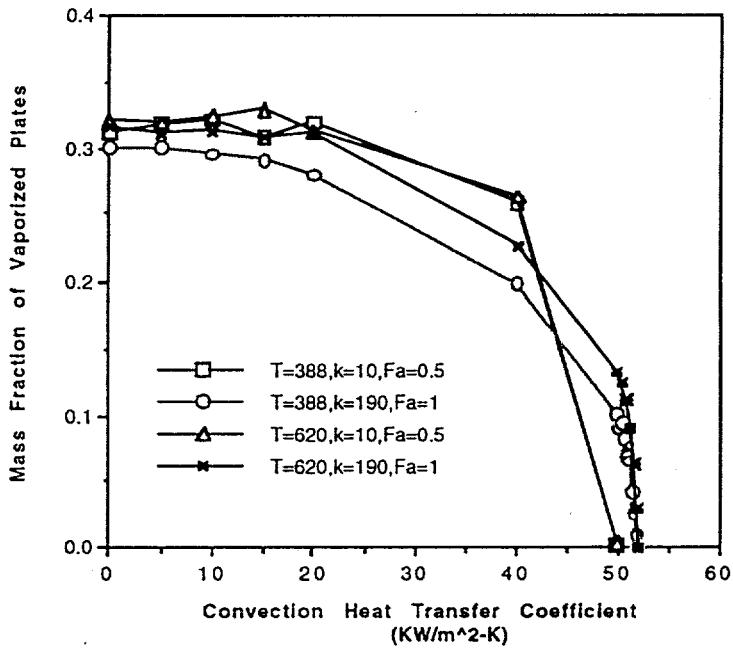

Fig. 8 Average mass fraction of vaporized plates.

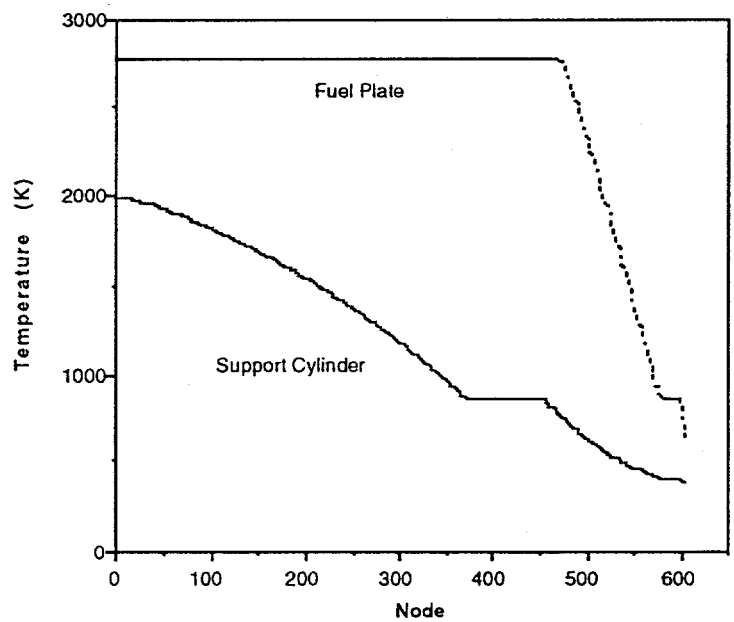

Fig. 9 Variation of node temperatures at the end of the calculations (six nodes correspond to one plate).

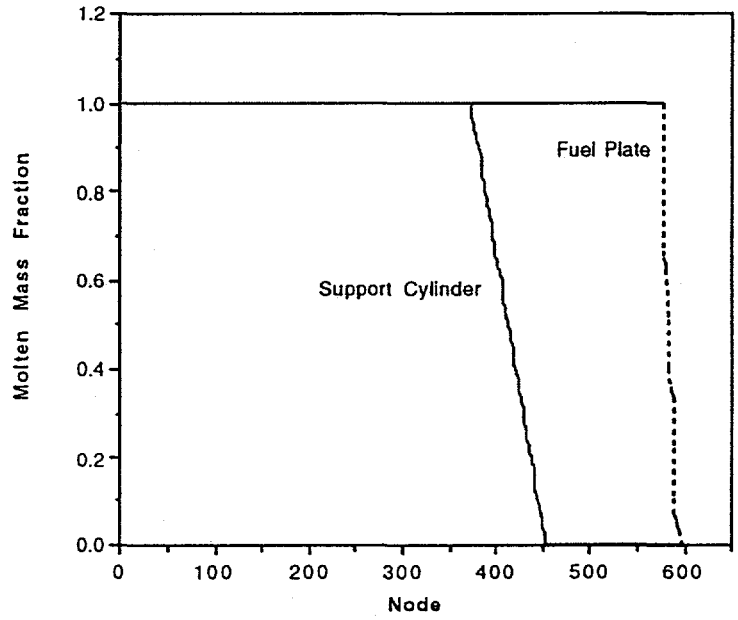

Fig. 10 Variation of molten mass fraction at the end of the calculations

not appropriate to assume that there is no fuel relocation/dispersal. Therefore, a parametric study has been performed to investigate the effect of molten fuel relocation/dispersal. The molten fuel (actually node) is forced to disappear once its temperature reaches a certain limit; one case with 1500 K, and the other with 863 K. A fuel melt temperature of 1500 K was selected as a fuel melt disappearance threshold, because that temperature is high enough to trigger the onset of aluminum ignition, as evidenced in past experiments [17]. 863 K was selected as the temperature at which molten fuel will either be swept upwards by the coolant or relocates downwards. This temperature is ~10K above aluminum melting temperature. Once the node at which the temperature increases above this threshold value disappears, we have to specify a new boundary condition to the inner node that was previously connected to the missing node. At this new boundary, the inner node may obtain more heat or lose heat depending on the situation. If extensive fuel ignition occurs, more energy will be added to the system under consideration through this boundary. If the relocation is due to coolant inertia, the system may loose heat to the coolant. For the current study, due to lack of knowledge on how this relocated node behaves, we assumed an adiabatic condition for this boundary. This assumption may not be too far from reality if we exclude the possibility of fuel ignition, since convective heat transfer in this channel is believed to be negligible. This is because the plate surface in this channel might be instantaneously covered by a vapor blanket upon coolant contact with the hot plate surface, along with reduced coolant velocity due to increased coolant channel flow area. For heat transfer at the damage propagation front, the same values of thermal conductivity and contact area between plates were used as for case 620-190-1 with no-melt removal. Results show that for both cases, the amount of damaged fuel was predicted to remain the same; that is 202 fuel plates. With an assumption of adiabatic boundary conditions, the heat flux at the damage propagation front was evaluated to be the same as that for the no-melt removal case. Therefore, damage propagation is predicted to proceed at the same speed, resulting in the same amount of fuel damage.

6. Summary and Conclusions

One-dimensional heat transfer calculations have been performed to investigate fuel plate damage propagation in the ANS reactor during a hypothetical coolant blockage event. The results provide useful insights into how various uncertain parameters affect the damage propagation. For the case with no heat transfer to the coolant, high thermal conductivity and high initial temperature for plate-2, and full thermal contact area of the swelled plates (e.g., the case is described in Fig. 6 as T=620, k=190, Fa=1), 202 plates, equivalent to about 30 kg of aluminum (202 plates x 0.1462 kg), are predicted as damaged at the end of 4 s. Also, it was found that the plate damage does not propagate if a 52 kW/m^2-K or larger heat transfer coefficient is provided to cool plate-2. The inclusion of side plates does not change the calculated number of damaged fuel plates. Instead, the energy content of those plates is reduced from about 180 MJ to 168.4 MJ. The difference (e.g., 11.6 MJ) has been transferred to the side plates. The mass of the side plates experiencing melting is estimated as 7.3 kg. This amount could contribute an additional chemical energy source of up to 130 MJ. A substantial portion of the side plates heated up to a temperature well beyond melting. Finally, it is cautioned that, if the plate damage was initiated in the lower fuel assembly, failure of the side plate may generate fragments that block the coolant channels of a downstream fuel assembly.

The present model represents an initial attempt at evaluating the highly complex aspects of ANS core damage propagation initiated by flow blockage. Shortcomings such as not accounting for fluid-structure interactions, core debris expulsion due to pressure buildup, plate rippling and buckling upon heatup, multidimensional effects, and absence of nuclear reactivity feedback will be addressed as necessary during the issue closure process wherein the ROAAM-type approach is being employed [18]. Nevertheless, the present model provides useful information on gauging the potential for core damage propagation in the absence of dynamic loads and sweepoff and evaluating the direction for further development and model enhancements.

7. References

[1] C. D. West, "The Advanced Neutron Source: A New Reactor-Based Facility for Neutron Research," Trans. Amer. Nuc. Soc. 61, 375 (June 1990).

[2] C. D. West, "Advanced Neutron Source Plant Design Requirements," ORNL/TM-11625 (May 1992).

[3] R. P. Taleyarkhan and S. H. Kim, "Severe Accident Risk Minimization Studies for the Advanced Neutron Source at the Oak Ridge National Laboratory," Proc. of the 5th International Workshop on Containment Integrity, Washington, D.C. (May 1992).

[4] C. Ramsey, "Probabilistic Risk Assessment of the Conceptual Design for the Advanced Neutron Source Reactor," ORNL/TM-12501 Draft (1993).

[5] S.H. Kim, et. al, "Study on Severe Accident Fuel Dispersion Behavior in the Advanced Neutron Source Reactor at Oak Ridge National Laboratory," ORNL/TM-12947, Oak Ridge National Laboratory (September 1995).

[6] R.P. Taleyarkhan, et. al., "Thermal-Hydraulics of Wave Propagation and Pressure Distribution Under Steam Explosion Conditions in the Advanced Neutron Source

Reactor," Proc. of the 7th International Meeting on Nuclear Reactor Thermal-Hydraulics (NURETH-7) Saratoga Springs, NY (September 1995).

[7] F.T. Binford, T.E. Cole and E.N. Cramer, "The High Flux Isotope Reactor Accident Analysis," ORNL-3573, Oak Ridge National Laboratory (April 1967).

[8] J.R. Kirkpatrick, "Estimate of Propagation of Melting in HFIR Fuel Plates Initiated by Blockage of Two Adjacent Channels," HFIR-CTD-91-JRK-15-2, Oak Ridge National Laboratory (May 1991)

[9] J. Freels, "Estimate of HFIR Core Damage Following a Core Blockage Based on RELAP5/Mod2.5/v3t with HFIR CHF Extensions," C-HFIR-92-023, Oak Ridge National Laboratory (June 1992)

[10] S.H. Kim, et. al., "A Parametric Model for Analyses of Melt Progression in U-Al Assemblies," Proc. of ANS Topical Meeting on the Safety, Status and Future of Non-Commercial Reactors and Irradiation Facilities, Boise, ID (October 1990).

[11] D.A. Anderson, J.C. Tannehill and R.H. Pletcher, "Computational Fluid Mechanics and Heat Transfer," McGraw-Hill Book Company (1984)

[12] K.W. Childs, "HEATING 7.2 User's Manual," ORNL/TM-12262, Oak Ridge National Laboratory (February 1993)

[13] R.P. Taleyarkhan, "Analysis and Modeling of Fission Product Release from Heated Uranium-Aluminum Plate Type Reactor Fuels," Nuclear Safety, Vol. 33-1 (1992).

[14] J.L. Snelgrove, et. al., "The Use of U_3Si_2 Dispersed in Aluminum in Plate-Type Fuel Elements for Research and Test Reactors," ANL/RERTR/TM-11, Argonne National Laboratory (October 1987).

[15] D.L. Selby, R.H. Harrington and P.B. Thompson, "Advanced Neutron Source (ANS) Project Progress Report, FY1994," ORNL-6821, Oak Ridge National Laboratory (January 1995).

[16] V. Georgevich, et. al., "Thermally Induced Dispersion Mechanisms for the U3Si2 Cermet Plate Type Fuel Under Rapid Transient Energy Deposition," Proc. of the 1995 National Heat Transfer Conference, Portland, OR (1995).

[17] L.S. Nelson, "Steam Explosions of Single Drops of Pure and Alloyed Molten Aluminum," Proc. of CSNI-FCI Specialist Meeting, Santa Barbara, CA (January 1993).

[18] T.G. Theofanous and H. Yan, "ROAAM: A Risk-Oriented Accident Analysis Methodology," Proc. of the International Conference on Probabilistic Safety Assessment and Management (PSAM), Beverly Hills, CA (February 1991).

Appendix A Nodal Temperature Evaluation*

For the surface node (massless) k=1, Eq. (2) becomes

$$C_{01}\left(T_0 - T_1\right) + C_{12}\left(T_2 - T_1\right) + Q_1 = 0 \tag{I.1}$$

At the surface, oxidation of the plate surface or radiation heat transfer may contribute to form Q_1 in Eq. (I.1). In a current modeling consideration, however, we assume that no energy generation is involved on the surfaces so that Q_1 becomes zero. Equation (I.1) can be rewritten for $T_0 = T_{f,L}$ (fluid temperature of flow channel on the left boundary of the plate)

$$T_1 = A_1\, T_2 + B_1 + D_1\, T_{f,L} \tag{I.2}$$

where constants in Eq. (I.2) are given as

$$\begin{aligned}
A_1 &= \frac{C_{12}}{U_1} \\
B_1 &= \frac{Q_1}{U_1} = 0 \\
D_1 &= \frac{C_{01}}{U_1} \\
U_1 &= C_{01} + C_{12} \\
Q_1 &= 0 \\
C_{01} &= h_L\, A_{01} = h_L\, w\, \Delta z \\
C_{12} &= \frac{\kappa_2\, A_{12}}{(\Delta x/2)} = \frac{2\,\kappa\, w\, \Delta z}{\Delta x}
\end{aligned} \tag{I.3}$$

where h_L is the convective heat transfer coefficient at this surface.

For interior nodes (k = 2, 3, ..., kmax-1), successive substitution of similar expressions into Eq. (2) gives

$$T_k = A_k\, T_{k+1} + B_k^* + D_k\, T_{f,L} \tag{I.4}$$

where

$$\begin{aligned}
A_k &= \frac{C_{k,k+1}}{U_k} \\
B_k^* &= \frac{1}{U_k}\left\{ Q_k + \frac{\left(m\, c_p\right)_k T_k^*}{\Delta t} + C_{k-1,k}\, B_{k-1}^* \right\} \\
D_k &= \frac{C_{k-1,k}\, D_{k-1}}{U_k}
\end{aligned} \tag{I.5}$$

---

* The numerical solution is obtained from Ref. [7] and was originally based on an unpublished work performed by V. Denny.

$$U_k = \frac{(m\,c_p)_k}{\Delta t} + C_{k-1,k}\left(1 - A_{k-1}\right) + C_{k,k+1}$$
$$Q_k = Q_{internal,k}$$
$$C_{k-1,k} = \frac{\kappa_{k-1}\,\kappa_k\,A_{k-1,k}}{\kappa_{k-1}\left(\frac{\Delta x_{k-1}}{2}\right) + \kappa_k\left(\frac{\Delta x_k}{2}\right)} = \frac{\kappa\,w\,\Delta z}{\Delta x}$$

At the surface (massless) node k=kmax, $T_{kmax+1} = T_{f,R}$, giving

$$T_{k\,max} = A_{k\,max}\,T_{f,R} + B^*_{k\,max} + D_{k\,max}\,T_{f,L} \tag{I.6}$$

To generalize the solution, Eq. (I.6) is rewritten as

$$T_{k\,max} = D_{k\,max}\,T_{f,L} + E_{k\,max}\,T_{f,R} + F^*_{k\,max} \tag{I.7}$$

where

$$\begin{aligned}
D_{k\,max} &= \frac{C_{k\,max-1,k\,max}\,D_{k\,max-1}}{U_{k\,max}} \\
E_{k\,max} &= \frac{C_{k\,max,k\,max+1}}{U_{k\,max}} \\
F^*_{k\,max} &= \frac{Q_{k\,max} + C_{k\,max-1,k\,max}\,B^*_{k\,max-1}}{U^*_{k\,max}} \\
U_{k\,max} &= C_{k\,max-1,k\,max}\left(1 - A_{k\,max-1}\right) + C_{k\,max,k\,max+1} \\
Q_{k\,max} &= 0 \\
C_{k\,max-1,k\,max} &= \frac{\kappa_{k\,max}\,A_{k\,max-1,k\,max}}{(\Delta x/2)} = \frac{2\,\kappa\,w\,\Delta z}{\Delta x} \\
C_{k\,max,k\,max+1} &= h_R\,A_{k\,max,k\,max+1} = h_R\,w\,\Delta z
\end{aligned} \tag{I.8}$$

where h_R is the convective heat transfer coefficient at this surface.

Back substitution of Eq. (I.7) into Eq. (I.4) for k = kmax-1, kmax-2, ..., 1, then gives the final form for the assembly nodal temperature distribution:

$$\begin{aligned}
T_k &= \left(A_k\,D_{k+1} + D_k\right)T_{f,L} + A_k\,E_{k+1}\,T_{f,R} + A_k\,F^*_{k+1} + B^*_k \\
&= D_k\,T_{f,L} + E_k\,T_{f,R} + F^*_k
\end{aligned} \tag{I.9}$$

Internal Distribution List

1.	D. H. Cook	12.	L. J. Ott
2.	W. G. Craddick	13.	D. L. Selby
3.	E. C. Fox	14.	D. B. Simpson
4.	V. Georgevich	15-17.	R. P. Taleyarkhan
5.	S. R. Greene	18.	C. D. West
6.	R. M. Harrington	19.	ORNL Patent Section
7.	S. A. Hodge	20.	Central Research Library
8-10.	S. H. Kim	21-22	Laboratory Records Department
11.	R. H. Morris		

External Distribution

23 S. Navarro-Valenti, 16 River Street #2, South Natick, MA 01760
24 J. Close, Idaho National Laboratories, P.O. Box 1625, EG&G, Idaho Falls, Idaho 83415
25. M. L. Corradini, Department of Nuclear Engineering, 1500 Johnson Drive, University of Wisconsin, Madison, Wisconsin, 53706-1687
26. M. L. Hyder, SRTC, Westinghouse Savannah River, Co., 1991 South Centennial Avenue, Bldg. 1, Aiken, South Carolina, 29803
27. R. T. Lahey, Nuclear Engineering and Engineering Physics, Rensselaer Polytechnic Institute, JEC 5048, Troy, New York, 12180-3590
28. M. Z. Podowoski, Nuclear Engineering and Engineering Physics, Rensselaer Polytechnic Institute, JEC 5048, Troy, New York, 12180-3590
29. J. Rsyskamp, Idaho National Laboratories, P.O. Box 1625, EG&G, Idaho Falls, Idaho 83415
30 -31. DOE, Office of Scientific and Technical Information, P.O. Box 62, Oak Ridge, Tennessee 37831
32. Sung-Tack Shin, KIDA, Chongryang P.O. Box 250, Togondae-mun-gu, Seoul, 130-650, South Korea
33. Kun-Joong Yoo, KAERI, P.O. Box 105, Yusung-gu, 305-600, South Korea
34. Tom King, U.S. Nuclear Regulatory Commission, MS T10-E37, Washington, D.C. 20555
35. Joe Donaghue, U. S. Nuclear Regulatory Commission, Washington, D. C. 20555
36. A. Drozd, U.S. Nuclear Regulatory Commission, Washington, D.C. 20555
37. T. Fuketa, Japan Atomic Energy Research Institute, Takai-Mura, Ibaraki-Ken, 319-11 Japan
38. J. Sugimoto,
39. T. G. Theofanous, University of California at Santa Barbara, Department of Chemical & Nuclear Engineering, Santa Barbara, California 93106